A hybrid elastic one-way propagator for strong-contrast media and its application to subsalt migration

Rui Yan[1], Ru-Shan Wu[1], Xiao-Bi Xie[1], and Dave Walraven[2] , [1]IGPP, Earth and Planetary Sciences Department, University of California, Santa Cruz; [2]Anadarko petroleum Corporation*

Summary

To overcome the weak scattering limitation of traditional one-way elastic propagator, we propose a hybrid elastic propagator for strong-contrast media, which combines the thin-slab propagator for weak perturbations and with the PO (physical optics) approximation at the irregular sharp boundaries. The hybrid propagator shuttles between wavenumber and space domain: wave propagation in wavenumber domain and heterogeneities interaction in space domain, rendering high efficiency and accuracy of the propagator. Numerical test using one simple salt model demonstrates the validity of the hybrid propagator. Finally the new propagator is applied to subsalt migration using synthetic data generated based on 2D Subsalt model.

Introduction

Subsalt exploration can be very challenging due to the issues posed by the often complex geometry of the salt bodies and the large impedance contrasts associated with salt/sediment interfaces. The large velocity contrast across the sedimentary/salt interfaces together with the frequently rugose character of these interfaces can prevent seismic waves from penetrating the salt body with sufficient strength to image subsalt structures. It is well known that converted-waves can penetrate a salt body and reach the blind zone of a P-wave survey. Some previous work using converted-wave imaging (Purnell, 1992; Kendall et al., 1998; Jones and Gasier, 1999; Wu et al., 2001) to improve the P-wave illumination utilized scalar wave propagators for both P- and S-waves. It is noted that scalar propagator for elastic wave propagation is dynamically incorrect. Preliminary studies of converted wave imaging using elastic wave propagator have also been reported (Wu et al., 2010).

Elastic thin-slab and elastic complex screen method (Wu, 1994; Wu and Xie, 1994; Xie and Wu, 1995, 2001, 2005; Wu and Wu, 2005; for a review, see Wu et al, 2007) are developed for one-way migration. It has its special feature and advantages in applying to seismic imaging. The extrapolated wavefields are vector wavefields but P and S modes are separated. These special features are especially useful for elastic wave imaging in terms of controlling migration artifacts and parameter inversion. Secondly, one-way wave method is much more efficient, often is orders of magnitude faster than the full wave method. However, those methods are based on perturbation theory. They can handle elastic perturbations only up to 30% (Wu and Wu, 2005) and may become instable beyond this limit. Although these methods can be useful in reservoir modeling and imaging, they fail to provide accurate wave propagation in strong heterogeneous media in which salt or basalt exists. To handle this specific case, we propose to solve the boundary problem by applying local reflection/transmission operator under the PO approximation (or Kirchhoff approximation) and combine it with thin-slab propagator for weak perturbations in the framework of one-way marching algorithm. In this study, we present the formulations for the theory on hybrid elastic one-way propagator and describe its three essential components in detail. Moreover, we conduct a numerical test to verify the accuracy and efficiency of the hybrid elastic one-way propagator and also use the Subsalt model to demonstrate its application to seismic imaging.

Theory

To handle the strongly heterogeneous media with sharp boundaries, such as salt or basalt inclusions, we divide the model into different domains along the sharp boundary (Figure 1). In each domain, the wave field can be computed with the representation integral:

$$\mathbf{u}(\mathbf{x}) = \int \mathbf{Q}(\mathbf{x}') \cdot \mathbf{G}(\mathbf{x};\mathbf{x}') d\Omega(\mathbf{x}') + \int \{[\hat{n} \cdot \boldsymbol{\sigma}(\mathbf{x}')] \cdot \mathbf{G}(\mathbf{x};\mathbf{x}') - \mathbf{u}(\mathbf{x}') \cdot [\hat{n} \cdot \boldsymbol{\Sigma}(\mathbf{x};\mathbf{x}')]\} dS(\mathbf{x}') \quad (1)$$

$$\mathbf{x}, \mathbf{x}' \in \Omega; \qquad S = \partial\Omega$$

where $\mathbf{u}(\mathbf{x})$ is the displacement field at point $\mathbf{X}$ within the volume Ω enclosed by surface S, $G(\mathbf{x};\mathbf{x}')$ is Green's displacement tensor (dyadic) and $\Sigma(\mathbf{x};\mathbf{x}')$ is Green's stress tensor (triadic). $\hat{n}$ is the surface normal as towards to the exterior of Ω. $\mathbf{u}(\mathbf{x}')$ and $\sigma(\mathbf{x}')$ are the displacement and stress on the surface; $\mathbf{Q}(\mathbf{x}')$ is body forces or equivalent body forces due to scattering. The volume integral term yields the contribution due to the sources inside Ω, while the surface integral term, that is, Kirchhoff integral, accounts for the energy communication between different domains. The traditional way to calculate the scattered wave in each domain is to solve the integral equation along the boundary. However, it involves huge computations because the interactions between all the boundary elements are considered. Following the spirit of the thin-slab propagator, we solve the problem iteratively in a one-way fashion. The resultant operator is called hybrid elastic one-way propagator.

Figure 1 schematically shows the realization of a typical hybrid propagator in strong heterogeneous medium with

DOI http://dx.doi.org/10.1190/segam2013-0712.1

sharp boundary. As the velocity model is sliced into thin slab, the sharp boundary is discretized into many boundary elements. The thin slab is separated into two domains: high velocity one and low velocity one by two boundary elements. Within each domain, the parameter variations (perturbations) are relatively weak. They are treated as volume scatterings and handled by thin-slab propagator. Besides the volume scatterings, each domain will admit internal reflections and transmissions from adjacent domains at the boundary elements. They together are called boundary scatterings. We assume that the boundary elements within one thin slab are decoupled from each other so that the reverberations between them are neglected. The displacement and traction fields of the boundary scatterings can be approximately calculated by applying reflection/transmission operator to the wave incident to the boundary element. It corresponds to the tangent plane approximation for smoothly curved boundary (Voronorich, 1989). When an incident wave enters a thin slab, it will interact with the volume heterogeneities as well as the boundary element in the current slab. The representation integral will give the scattered wave which will be added to the incident wave at the exit of the thin slab. Based on the one-way propagation principle, the wavefields are updated iteratively step-by-step in the forward direction with no consideration of the backward scatterings.

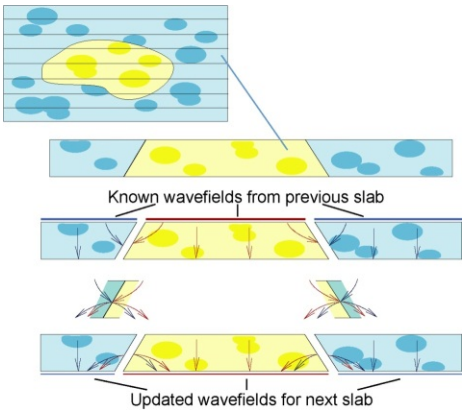

Figure 1. Schematic illustration of the hybrid elastic one-way propagator.

In the subsection, we will describe three critical components of migration algorithms: thin-slab propagator for weak volume scatterings, background propagation, and reflection/transmission operator for sharp boundary scatterings.

1. Thin-slab propagator for weak volume scatterings

When several domains exist in a velocity model, the wave propagation in each domain will be handled separately with traditional thin-slab propagator. Different domains have different background velocities, so that the weak perturbations assumptions of thin-slab propagator can be guaranteed in each domain. The interaction with the weak heterogeneities will be calculated by the local Born approximation

$$\mathbf{u}_V^{P/S(i)}\left(\mathbf{K}_T, z_j\right) = \int_{z_{j-1}}^{z_j} dz \int d^2\mathbf{x}_T \mathbf{Q}_0\left(\mathbf{x}_T, z\right) \cdot \mathbf{G}_0^{P/S(i)}\left(\mathbf{K}_T, z_i; \mathbf{x}_T, z\right), \quad \left(\mathbf{x}_T, z\right) \in \Omega_i \tag{2}$$

where Ω_i is domain i, and $\mathbf{Q}_0\left(\mathbf{x}_T, z\right)$ is the equivalent body force due to the interaction of perturbations and incident fields. For isotropic media,

$$\mathbf{Q}_0\left(\mathbf{x}_T, z\right) = \delta\rho\left(\mathbf{x}_T, z\right)\omega^2\mathbf{u}_0\left(\mathbf{x}_T, z\right) + \nabla\cdot\left[\delta\lambda\left(\mathbf{x}_T, z\right)\left|\varepsilon_0\left(\mathbf{x}_T, z\right)\right|\mathbf{I} + 2\delta\mu\left(\mathbf{x}_T, z\right)\varepsilon_0\left(\mathbf{x}_T, z\right)\right] \tag{3}$$

where ρ is the density; λ and μ are the Lame constants, $\mathbf{I}$ is the unit tensor; $\mathbf{u}_0\left(\mathbf{x}_T, z\right)$ and $\varepsilon_0\left(\mathbf{x}_T, z\right)$ are the space-domain displacement and strain field of incident wave, respectively;

$$G_0^P\left(\mathbf{K}_T, z_i; \mathbf{x}_T, z\right) = \frac{ik_\alpha^2}{2\rho_0\omega^2\gamma_\alpha}\hat{k}_\alpha\hat{k}_\alpha e^{-i\mathbf{K}_T x_T + i\gamma_\alpha\left(z_i - z\right)}, \tag{4}$$

$$G_0^S\left(\mathbf{K}_T, z_i; \mathbf{x}_T, z\right) = \frac{ik_\beta^2}{2\rho_0\omega^2\gamma_\beta}\left(\mathbf{I} - \hat{k}_\beta\hat{k}_\beta\right)e^{-i\mathbf{K}_T x_T + i\gamma_\alpha\left(z_i - z\right)}, \tag{5}$$

are the background Green' tensor of displacement, in which $\mathbf{k}_\alpha = \left(\mathbf{K}_T, \gamma_\alpha\right)$ and $\mathbf{k}_\beta = \left(\mathbf{K}_T, \gamma_\beta\right)$ are the P and S wavenumber vectors respectively, with $\mathbf{K}_T$ as the horizontal wavenumber, γ_α and γ_β as vertical wavenumbers, $\hat{\mathbf{k}}_\alpha$ and $\hat{\mathbf{k}}_\beta$ as the unit vectors for P and S waves, respectively.

2. Background propagations

The free propagations (background propagations) in the hybrid propagator are expressed as phase shifts in wavenumber domain:

$$\mathbf{u}_0^{P/S(i)}\left(\mathbf{K}_T, z\right) = e^{i\gamma_{\alpha,\beta}\left(z - z_{j-1}\right)}\int d^2\mathbf{x}_T e^{-i\mathbf{K}_T\mathbf{x}_T}\mathbf{u}_0^{P/S(i)}\left(\mathbf{x}_T, z_{j-1}\right), \tag{6}$$

$\left(\mathbf{x}_T, z_{j-1}\right) \in \Omega_i$, where Ω_i is domain i.

3. Transmission/reflection operators on the boundary elements

Boundary scatterings are formulated in different way from volume scatterings in the thin slab. To compute the boundary scattering, we make a tangent plane approximation (Voronovich, 1999) which assumes the boundary surface is smoothly curved so that the reflection/transmission coefficients defined for an infinite plane surface can be applied locally at each surface element.

DOI http://dx.doi.org/10.1190/segam2013-0712.1

A hybrid elastic one-way propagator

We focus our attention to one boundary element which separates the medium into upper and lower ones. Regardless of their real domain numbers, we set the index for the upper medium as 1 and the lower medium as 2. The incident waves of the upper and lower medium are given from the output of previous thin slab as $\mathbf{U}_{0,1}^{P/S}(\mathbf{K}_T)$ and $\mathbf{U}_{0,2}^{P/S}(\mathbf{K}_T)$ in wavenumber domain. These incident waves include the scatterings of the previous boundary elements and the contributions from underneath are ignored. To accurately calculate the energy partition at the boundary element, we transform the displacement of the incident waves at the upper and lower mediums from the Cartesian coordinate to $\tilde{\mathbf{U}}_{0,1}^{P/S}(\mathbf{K}_T)$ and $\tilde{\mathbf{U}}_{0,2}^{P/S}(\mathbf{K}_T)$ defined in the local boundary coordinate (with horizontal axis parallel to the tangent of the local boundary).

In the local boundary coordinate, reflection/transmission coefficients are applied to the incident wave to get the reflected and transmitted waves:

$$\begin{bmatrix} \tilde{\mathbf{U}}_1^P(\mathbf{K}_T) \\ \tilde{\mathbf{U}}_1^S(\mathbf{K}_T) \\ \tilde{\mathbf{U}}_2^P(\mathbf{K}_T) \\ \tilde{\mathbf{U}}_2^S(\mathbf{K}_T) \end{bmatrix} = \begin{bmatrix} R_{11}^{PP} & R_{11}^{SP} & T_{21}^{PP} & T_{21}^{SP} \\ R_{11}^{PS} & R_{11}^{SS} & T_{21}^{PS} & T_{21}^{SS} \\ T_{12}^{PP} & T_{12}^{SP} & R_{22}^{PP} & R_{22}^{SP} \\ T_{12}^{PS} & T_{12}^{SS} & R_{22}^{PS} & R_{22}^{SS} \end{bmatrix} \begin{bmatrix} \tilde{\mathbf{U}}_{0,1}^P(\mathbf{K}_T) \\ \tilde{\mathbf{U}}_{0,1}^S(\mathbf{K}_T) \\ \tilde{\mathbf{U}}_{0,2}^P(\mathbf{K}_T) \\ \tilde{\mathbf{U}}_{0,2}^S(\mathbf{K}_T) \end{bmatrix}, \quad (7)$$

where R and T are reflection and transmission coefficients calculated by Zoeppritz's equation (Aki and Richards, 1980). The coefficients are dependent on the horizontal slowness in the local boundary coordinate. The first and second subscripts of the coefficients are the medium indexes. The superscripts of the coefficients specify the wave types in the upper and lower medium, respectively. $\tilde{\mathbf{U}}_I^{P/S}, I = 1,2$ is the displacement of the boundary scattering which is the sum of the internal reflected wave and the transmitted wave from the other domain.

The traction of the boundary scattering $\tilde{\mathbf{T}}_I^{P/S}(\mathbf{K}_T)$ can be calculated from the displacement $\tilde{\mathbf{U}}_I^{P/S}(\mathbf{K}_T)$ by the constitutive equation in wavenumber domain. And then we transform both displacement and traction into space domain and back to the Cartesian coordinate. We pick the values at the boundary element and return to the domain they belongs to as $\mathbf{U}^{P/S(i)}(\mathbf{x}_T, z)$ and $\mathbf{T}^{P/S(i)}(\mathbf{x}_T, z)$.

The scattered waves due to the boundary element at the slab exit can be calculated by Kirchhoff integral in the horizontal wavenumber domain (Wu, 1989)

$$\mathbf{u}_B^{P/S(i)}(\mathbf{K}_T, z_j) = \int_L \Big[\mathbf{T}^{P/S(i)}(\mathbf{x}_T, z) \cdot \mathbf{G}_0^{P/S(i)}(\mathbf{K}_T, z_j; \mathbf{x}_T, z) - \mathbf{U}^{P/S(i)}(\mathbf{x}_T, z) \cdot \mathbf{\Gamma}_0^{P/S(i)}(\mathbf{K}_T, z_j; \mathbf{x}_T, z, \hat{n}) \Big] dS, \quad (8)$$

where i is the domain number; L is the boundary segment which separates upper and lower medium. where

$$\Gamma_0^P(\mathbf{K}_T, z_i; \mathbf{x}_T, z, \hat{n}) = \frac{-k_\alpha^3}{2\rho_0 \omega^2 \gamma_\alpha} \times \Big[\lambda \hat{k}_\alpha \hat{n} + 2\mu (\hat{n} \cdot \hat{k}_\alpha) \hat{k}_\alpha \hat{k}_\alpha \Big] e^{-i\mathbf{K}_T x_T + i\gamma_\alpha (z_i - z)}, \quad (9)$$

$$\Gamma_0^S(\mathbf{K}_T, z_i; \mathbf{x}_T, z, \hat{n}) = \frac{-k_\beta^3}{2\rho_0 \omega^2 \gamma_\beta} \times \mu \Big[(\hat{n} \cdot \hat{k}_\beta) \mathbf{I} + \hat{k}_\beta \hat{n} - 2(\hat{n} \cdot \hat{k}_\beta) \hat{k}_\beta \hat{k}_\beta \Big] e^{-i\mathbf{K}_T x_T + i\gamma_\alpha (z_i - z)}, \quad (10)$$

are the background Green's tractions.

At the exit of each thin-slab, the total field is composed of three parts: the incident (free-propagated) wave $\mathbf{u}_0^{(i)}$, the scattered field by volume heterogeneities $\mathbf{u}_V^{(i)}$ and the boundary scattered field $\mathbf{u}_B^{(i)}$

$$\mathbf{u}^{P/S(i)}(\mathbf{x}_T, z_j) = \frac{1}{4\pi^2} \int d^2 \mathbf{K}_T e^{i\mathbf{K}_T \mathbf{x}_T} \Big[\mathbf{u}_0^{P/S(i)}(\mathbf{K}_T, z_j) + \mathbf{u}_V^{P/S(i)}(\mathbf{K}_T, z_j) + \mathbf{u}_B^{P/S(i)}(\mathbf{K}_T, z_j) \Big], \ (\mathbf{x}_T, z_j) \in \Omega_i \quad (11)$$

where Ω_i is domain i.

Numerical tests

First we test the elastic one-way propagator using a salt with a wedge shape embedded in a homogeneous media. Figure 2 illustrates the velocity model with elastic parameters. The source is a 15 Hz Ricker wavelet and located in the center of the model. In this simple case, the PO approximation is expected to work the best. Illustrated in the upper panel of Figure 3 are the horizontal and vertical displacements calculated by elastic one-way propagator. Compared with the snapshots calculated from full-wave finite difference (FD) (the lower panel of Figure 3), the transmitted wavefront of the elastic one-way propagator matches with them very well. The energy partition at the interface is almost the same as full-wave FD.

Next we move on to a more complex model – 2D velocity profile simulating the Subsalt model (Figure 4). On top of the model is a water layer. FD cannot solve the fluid-solid problem very well. On the contrary, the hybrid propagator can do a good job to handle the interface. The model is divided into three different domains: water, sediment and salt. Each domain has its own background and perturbation parameters. We design an observation system and conduct

DOI http://dx.doi.org/10.1190/segam2013-0712.1

a seismic experiment. The acquisition system was comprised of 301 shots from 7000 m to 37000 m with an interval of 100 m. Each shot was recorded by a line of receivers with double-spread configuration. The number of receivers was 561 and the maximal offset is 7000 m. Both sources and receivers are located on the water surface. The recorded data are pressure only simulating a hydrophone response. The source is a 15 Hz Ricker wavelet and the total recording time is 12 s with a time interval of 0.01 s. The synthetic data were modeled by the Tesseral 2D application package using a FD approach. We migrate the seismic data with the hybrid one-way propagator and obtain the PP, PS, SP and SS images. Here we only show PP image in Figure 5 because it has the highest signal-to-noise ratio. From the migration image, a large portion of subsalt reflectors can be clearly identified, except the section with very large dips. There are some migration artifacts near the true images due to multiples and cross-talk. Preprocessing the seismic data will help to improve the quality of the migration image.

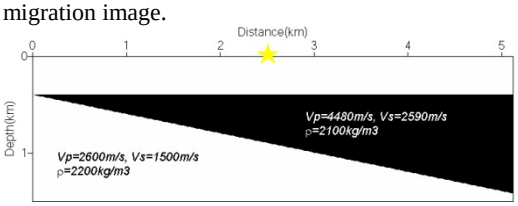

Figure 2. An elastic salt model. The elastic parameters and shot location are indicated in the figure.

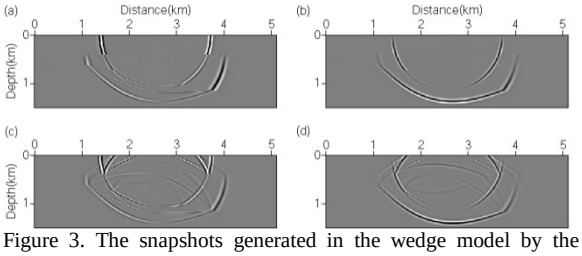

Figure 3. The snapshots generated in the wedge model by the hybrid elastic propagator (upper panel) and finite difference (lower panel). The horizontal components are shown on the left and the vertical components are shown on the right.

Conclusions

We developed the theory and method of a hybrid elastic one-way operator which combines the elastic thin-slab propagator in weakly heterogeneous media and reflection/transmission operators at the sharp boundaries. The accuracy and efficiency of the dual-domain, depth-marching propagator are validated by a simple numerical example. The application of the propagator to seismic imaging is demonstrated on Subsalt model and three subsalt reflectors are shown clearly in the resulted migration image.

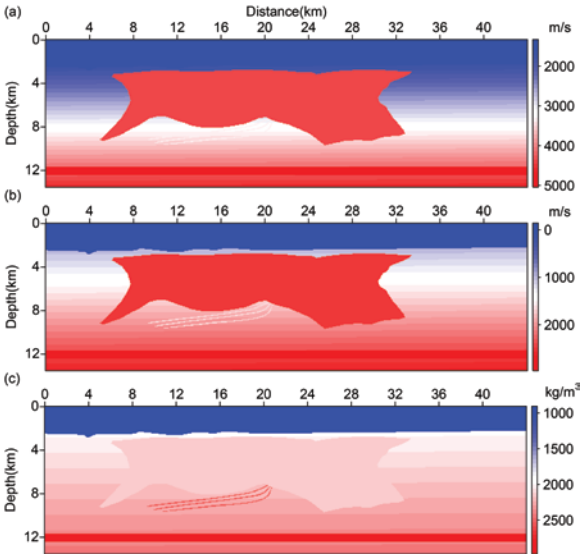

Figure 4. The 2D Subsalt model: (a) P-wave velocity; (b) S-wave velocity and (c) density.

Acknowledgements

The research work is funded by DEEPSTAR project. The authors acknowledge the support from WTOPI consortium at UC Santa Cruz. The authors thank Anadarko for providing the 2D Subsalt model and the help from the technicians in Tetrale Company in generating the synthetic data for the model. The authors appreciate the helpful discussions with Zengxi Ge and Yingcai Zheng.

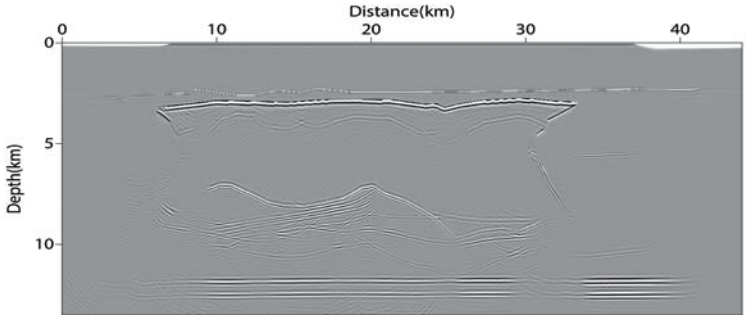

Figure 5. The PP image of 2D Subsalt model generated by elastic one-way propagator.

DOI http://dx.doi.org/10.1190/segam2013-0712.1

http://dx.doi.org/10.1190/segam2013-0712.1

EDITED REFERENCES

Note: This reference list is a copy-edited version of the reference list submitted by the author. Reference lists for the 2013 SEG Technical Program Expanded Abstracts have been copy edited so that references provided with the online metadata for each paper will achieve a high degree of linking to cited sources that appear on the Web.

REFERENCES

Aki, K., and P. G. Richards, 1980, Quantitative seismology: Theory and methods, W. H. Freeman and Co.

Jones, N., and J. Gaiser, 1999, Imaging beneath high-velocity layers: 68th Annual International Meeting, SEG, Expanded Abstracts, 713–716.

Kendall, R. R., S. H. Gray, and G. E. Murphy, 1998, Subsalt imaging using prestack depth migration of converted waves: Mahogany Field, Gulf of Mexico: Annual International Meeting, SEG, Expanded Abstracts, 2052–2055.

Purnell, G. W., 1992, Imaging beneath a high-velocity layer using converted wave: Geophysics, **57**, 1444–1452, http://dx.doi.org/10.1190/1.1443212.

Voronovich, A. G., 1999, Wave scattering from rough surface: Springer-Verlag.

Wu, R. S., 1989, Representation integrals for elastic wave propagation containing either the displacement term or the stress term alone: Physical Review Letters, **62**, no. 5, 497–500, http://dx.doi.org/10.1103/PhysRevLett.62.497.

Wu, R. S., 1994, Wide-angle elastic wave one-way propagation in heterogeneous media and an elastic wave complex-screen method: Journal of Geophysical Research, **99**, B1, 751–766, http://dx.doi.org/10.1029/93JB02518.

Wu, R. S., H. Guan, and X. Y. Wu, 2001, Imaging steep subsalt structure using converted wave paths: Presented at the 71st Annual International Meeting, SEG.

Wu, R. S., and X. B. Xie, 1994, Multiscreen back propagator for fast 3D elastic prestack migration: Mathematical Methods in Geophysical Imaging II SPIE, **2301**, 181–193, http://dx.doi.org/10.1117/12.187491.

Wu, R. S., X. B. Xie, and X. Y. Wu, 2007, One-way and one-return approximations for fast elastic wave modeling in complex media, *in* R. S. Wu and V. Maupin, eds., Advances in wave propagation in heterogeneous earth: Elsevier, 266–323.

Wu, R. S., R. Yan, X. B. Xie, and D. Walraven, 2010, Elastic converted-wave path migration for subsalt imaging: 80th Annual International Meeting, SEG, Expanded Abstracts, **29**, 3176–3180.

Wu, X. Y., and R. S. Wu, 2006, AVO modeling using elastic thin-slab method: Geophysics, **71**, no. 5, C57–C67, http://dx.doi.org/10.1190/1.2227520.

Xie, X. B., and R. S. Wu, 1995, A complex-screen method for modeling elastic wave reflections: 65th Annual International Meeting, SEG, Expanded Abstracts, 1269–1272.

Xie, X. B., and R. S. Wu, 2001, Modeling elastic wave forward propagation and reflection using the complex screen method: The Journal of the Acoustical Society of America, **109**, no. 6, 2629–2635, http://dx.doi.org/10.1121/1.1367248.

Xie, X. B., and R. S. Wu, 2005, Multicomponent prestack depth migration using elastic screen method: Geophysics, **70**, no. 1, S30–S37, http://dx.doi.org/10.1190/1.1852787.